NATIONAL ADVISORY COMMITTEE FOR AERONAUTICS

TECHNICAL NOTE 3776

HEAT-TRANSFER MEASUREMENTS ON TWO BODIES OF REVOLUTION AT A MACH NUMBER OF 3.12

By John R. Jack and N. S. Diaconis

Lewis Flight Propulsion Laboratory
Cleveland, Ohio

Washington
October 1956

NATIONAL ADVISORY COMMITTEE FOR AERONAUTICS

TECHNICAL NOTE 3776

HEAT-TRANSFER MEASUREMENTS ON TWO BODIES OF REVOLUTION AT A MACH NUMBER OF 3.12

By John R. Jack and N. S. Diaconis

SUMMARY

Local rates of heat transfer were obtained from a cone cylinder and a parabolic-nosed cylinder at a Mach number of 3.12. Data were obtained for Reynolds numbers up to 12×10^6 based on body length for heated and cooled surfaces.

The laminar-heat-transfer coefficients obtained from the conical portion of the cone cylinder agree closely with theory at all temperature levels when corrected for the axial temperature distribution. Experimentally and analytically, there seems to be no significant effect of temperature level on the heat-transfer coefficient. The laminar data obtained from the parabolic-cylinder model agree closely with theory when the axial pressure distribution is considered and the data are corrected for the axial temperature distribution.

INTRODUCTION

The aerodynamic heating problem is being investigated at the NACA Lewis laboratory in order to supply the designer of high-speed aircraft and missiles with quantitative heat-transfer and boundary-layer-transition data. These two phases of the aerodynamic heating problem, the value of heat-transfer coefficients and the location of the boundary-layer transition, are, of course, interrelated. The order of magnitude of the heat-transfer rate depends on whether the boundary layer is laminar or turbulent; whereas, the location of transition is influenced by the amount of heat transferred.

Studies of the laminar and turbulent heat-transfer rates on bodies of revolution are presented in references 1 to 3. In reference 1, which is a summary paper of five investigations, laminar-heat-transfer coefficients are reported for a heated cone and a parabolic-arc body, and for a cooled cone at Mach numbers between 1.5 and 2.2. The experimental data agree closely with the theories of Crocco (ref. 4) and Chapman and

Rubesin (ref. 5). Eber (ref. 2) obtained heat-transfer rates for a cone cylinder at local Mach numbers ranging from 0.88 to 4.65. Again, the experimental data are well represented by the isothermal theory of Crocco. The data presented in references 1 and 2 were obtained at temperatures near the equilibrium temperature. Heat-transfer measurements made by DeCoursin, Bradfield, and Sheppard (ref. 3) on various cones and parabolic-arc configurations at ratios of wall-to-local-free-stream temperature ranging from 2.0 to 4.8 are the only current wind-tunnel measurements available for a range of surface-temperature levels. The laminar data obtained on all models agree closely with the theory of Chapman and Rubesin (ref. 5). However, the turbulent data obtained from the cones did not agree closely with the theory of Van Driest (ref. 6).

Previously, the effects of surface temperature on transition have been evaluated only at relatively low Mach numbers. Reference 7 reports the effects of surface temperature and pressure gradient on transition under the condition of large heat transfer. The models considered were a 9.5°-apex-angle cone cylinder and a parabolic-nosed cylinder, each with a nose fineness ratio of 6.

In this investigation, heat-transfer coefficients for the same two models at zero angle of attack are reported for wall-to-free-stream static-temperature ratios ranging from 1.0 to 4.4.

APPARATUS AND PROCEDURE

The investigation was conducted in the Lewis 1- by 1-foot supersonic wind tunnel, which operates at a Mach number of 3.12. Tests were made at various Reynolds numbers ranging from 2×10^6 to 12×10^6 based on model length. The tunnel stagnation dew point was about -35° F at all times. Further details concerning this facility may be found in reference 7.

The dimensions and thermocouple locations of the models used to obtain the heat-transfer data are shown in figure 1. Both models were constructed from a nickel alloy with a wall thickness of approximately 1/16 inch. The cone cylinder was made of monel, whereas the parabolic-nosed cylinder was fabricated from "K" monel. The maximum surface roughness on each was less than 16 microinches. Each model was instrumented with calibrated copper-constantan thermocouples of 30-gage wire. A typical tunnel installation is shown in figure 2. The theoretical wall-pressure distributions for the two models are presented in figure 3. These distributions were calculated using the second-order theory presented in reference 8.

Heat-transfer data were obtained by utilizing the transient technique described in detail in reference 7. Transient temperature

distributions were obtained from data recorded on multiple-channel oscillographs. Data obtained prior to 30 seconds were not reduced. A typical temperature history for the cooled cone is presented in figure 4. This distribution is, incidentally, similar to that obtained on a heat-capacity cooled vehicle.

DATA REDUCTION

The general equation describing the transient heat-transfer process for a cone having a thin wall is, with the local heat-transfer rate q per unit area,

$$q_{total} = q_{convection} + q_{conduction\ in\ skin} + q_{radiation} + q_{conduction\ to\ inside\ of\ model}$$

or, more explicitly,

$$\rho_b c_{p,b} \tau \frac{\partial T_w}{\partial t} = \left[h(T_{ad} - T_w) \right] + \left[k_b \tau \left(\frac{\partial^2 T_w}{\partial X^2} + \frac{1}{X} \frac{\partial T_w}{\partial X} \right) \right] + q_{radiation} + q_{conduction\ to\ inside\ of\ model} \tag{1}$$

(All symbols are defined in appendix A.)

The magnitudes of the radiation and conduction terms in equation (1) were investigated in appendix B using experimental data. In all cases, the radiation and conduction terms were less than 2 percent of the total heat transferred and were therefore disregarded. When these terms are eliminated from equation (1), the expression for the local heat-transfer coefficient h becomes

$$h = \frac{\rho_b c_{p,b} \tau \frac{dT_w}{dt}}{T_{ad} - T_w} \tag{2}$$

When the experimental values of h were determined, the corresponding values of free-stream Stanton number were computed from

$$St_0 = \frac{h}{\rho_0 c_{p,a} u_0}$$

The time rates of change of temperature were found from faired curves by using either a five-point numerical differentiation or an

optical differentiator. The optical differentiator was similar to that described in reference 9 plus the added provision for attaching it to a drafting machine thus permitting a direct reading of the tangent angle. Slopes obtained by both methods were found to have a maximum deviation of ±3 percent from the slope of an analytical curve. For most of the data presented herein, the optical differentiator was used.

The adiabatic wall temperature T_{ad} needed to evaluate the heat-transfer coefficient is usually obtained with the model at the zero heat-transfer condition. However, because of the effect of heat transfer, the location of transition varied considerably from that obtained at adiabatic wall conditions (see ref. 7). For this reason, the recovery temperature was taken as

$$T_{ad} = T_1 + \eta(T' - T_1)$$

where the temperature recovery factor $\eta = \sqrt{Pr}$ for laminar flow and $\eta = \sqrt[3]{Pr}$ for turbulent flow, with the Prandtl number Pr evaluated at adiabatic wall temperature. In the cases that could be checked, the experimental recovery temperatures agreed closely with those calculated using the theoretical recovery factor.

A knowledge of the variation of specific heat with temperature of the model material is required to apply equation (2) over a large temperature range. The specific heat of monel has been established over the temperature range of this investigation (refs. 10 and 11); however, the specific heat of "K" monel is unknown. Since the composition of "K" monel and monel are very nearly the same (table I), it was anticipated that the respective specific heats would be approximately equal. To verify this assumption, the theoretical specific heats for monel and "K" monel were evaluated using Kopp's rule (ref. 12) and compared with the experimental values for monel. Figure 5 shows the result of this comparison. The theoretical specific heats obtained for both alloys agree closely with the experimental values for monel between 150° and 500° R. As a result, the experimental specific heats for monel were used to reduce the data. The disagreement that exists between theory and experiment at the high temperatures is due to the inadequacy of the theory in this temperature range.

The accuracy of the experimental data was determined from the estimated uncertainties of the individual measurements entering into the determination of the final results. (Appendix B explains the radiation and

conduction errors.) The estimated uncertainties of the basic measurements are given in the following table:

Wall thickness, τ, percent	±1
Slope, dT_w/dt, percent	±3
Specific heat of model wall material, $c_{p,b}$, percent	±3
Model wall temperature, T_w, °R:	
High-temperature range	±1
Low-temperature range	±3
Total pressure, P', percent	±0.3
Total temperature, T', °R	±2

Since the model wall thickness enters directly into the heat-transfer calculation (see eq. (2)), the models were cut apart and the wall thickness at the thermocouple locations measured accurately. This accounts for the very small uncertainty in the wall thickness. The relative error of any parameter was determined from the uncertainies of its components. A maximum relative error of ±16 percent was found for the Stanton number. In most instances, however, the data are so consistent and vary so smoothly that the relative error is believed to be less than this value.

At very low model temperatures (120° to 250° R), two condensation films appeared on the model surface and subsequently evaporated as the model temperature increased. An observer watching this phenomenon would first see one film form and evaporate, and then the same process repeated for the second film. Thus, the measured temperatures were subject to error since the model was not receiving all the heat being transferred. In an attempt to ascertain the order of magnitude of the condensation error, several calculations were made and are presented in appendix C. The calculations indicate that the condensation phenomenon did not have an appreciable effect on the determination of heat-transfer coefficients.

THEORETICAL CONSIDERATIONS

In this section, a brief summary of the presently available laminar and turbulent theories which the designer has at his disposal is provided.

Laminar Heat Transfer

Eckert (ref. 13) indicates that constant Prandtl number solutions (e.g., Chapman and Rubesin, ref. 5) agree well with the solutions allowing variation of the Prandtl number through the boundary layer (refs. 4 and 14 to 16) when the fluid properties are evaluated at a reference

temperature. As a result, the isothermal theory of Chapman and Rubesin, based on Eckert's reference temperature and converted by Mangler's transformation (ref. 17), has been chosen as a basis for comparison with the experimental data for the cone-cylinder model. With the exception of the Chapman and Rubesin theory, all the aforementioned theories are limited to the flow over isothermal surfaces. However, all of them may be used if the effects of an axial temperature distribution are accounted for by the solution of either Chapman and Rubesin or Lighthill (ref. 18).

The importance of a variable surface temperature is illustrated by considering a wall-temperature distribution that varies linearly with distance from the leading edge and assuming that the leading edge is at the adiabatic wall temperature. Theoretically, the heat-transfer coefficient is about 65 percent larger than that obtained for a constant wall temperature under the same conditions. If the wall temperature varies as the square of the distance from the leading edge, the difference is 100 percent. It is interesting to note that the changes in heat-transfer coefficient due to such a temperature gradient depend only on the form of the gradient, and not on its magnitude. The effect on heat-transfer rate, on the other hand, depends strongly on the magnitude of the temperature gradient. Thus, the temperature variation along the surface of a vehicle must be considered for an accurate interpretation of heat-transfer data obtained from a nonisothermal surface when the boundary layer is laminar.

The most convenient method of accounting for a temperature distribution in a three-dimensional laminar flow is to transform it to the equivalent two-dimensional distribution by Mangler's transformation (ref. 17) and apply Lighthill's theory, which states

$$\frac{h}{\bar{h}} = \frac{T(0) - T_{ad}}{T(x) - T_{ad}} + \frac{x^{1/4}}{T(x) - T_{ad}} \int_0^x \frac{\frac{dT}{d\xi}\, d\xi}{\left(x^{3/4} - \xi^{3/4}\right)^{1/3}} \qquad (3)$$

where $T(0)$ is the leading-edge temperature, ξ is a dummy variable representing distance measured in the x-direction, and $\bar{h}$ is the isothermal heat-transfer coefficient. For any sharp-nosed body of revolution, the leading edge will rapidly approach the adiabatic wall temperature because the rate of heat transfer near the leading edge is very large. Thus, the first term on the right side of equation (3) becomes zero when x is not zero. A sample axial temperature distribution on the cone is presented in figure 6. Also included in figure 6 is the equivalent flat-plate temperature distribution used in applying the Lighthill modification. The figure illustrates how the experimental data were faired to the adiabatic wall temperature for computation of temperature gradient effects.

Chapman and Rubesin (ref. 5), in their solution of the boundary-layer equations, considered a surface temperature distribution that is expressible as a polynomial in the distance from the leading edge. However, the Lighthill method is considerably simpler to apply than that of Chapman and Rubesin because the surface temperature distribution need not be expressed as a polynomial, but may be approximated by linear segments. Thus, for each segment, the derivative of temperature in the integrand of equation (3) is a constant and the integral may be evaluated. Although Lighthill's theory is for incompressible flow, a comparison of the two theories for a temperature distribution of the type $T_w - T_{ad} = ax^n$ shows agreement within 3 percent for values of n up to 10. The practical application of Lighthill's theory is discussed in detail in reference 19.

The analysis of Cohen and Reshotko (ref. 20) was used for comparison with the experimental data obtained on both the cylindrical section of the cone-cylinder and the parabolic-nosed-cylinder models. Although this theory is derived for a constant wall temperature, it does permit arbitrarily large pressure gradients and heat transfer. However, as was discussed previously, the heat transfer to a body is sensitive to surface temperature gradients so that the theory of reference 20 is not expected to correlate closely with the uncorrected experimental data. It might be anticipated, however, that the effect of the temperature gradient could be approximately accounted for by transforming the temperature distribution to the equivalent two-dimensional distribution and then using Lighthill's theory.

Turbulent Heat Transfer

Many assumptions are incorporated in the existing theoretical analyses of the turbulent boundary layer. Furthermore, mixed laminar and turbulent flows have not been considered, necessitating an arbitrary choice of the origin of the turbulent boundary layer. Also, none of the current compressible theories account for a temperature distribution downstream of the transition region. In view of the foregoing, the experimental turbulent-heat-transfer coefficients are not expected to agree well with existing turbulent-boundary-layer theory.

Transient Effects

Although the preceding discussion is strictly applicable to steady-state flow, it is possible to compare the experimental data with the theories discussed if certain reservations are made. The restriction imposed is that the time rate of change of temperature appearing in the energy equation must be small compared with the terms retained; then the

boundary-layer flow at any time is well described by the steady-state solutions. An order of magnitude analysis of the contribution of the time rate of change of temperature indicates that, for the data presented herein, it is quite small.

RESULTS AND DISCUSSION

Experimentally determined Stanton numbers for the cone-cylinder model at average wall-to-free-stream temperature ratios of 1.0 and 4.0 are presented in figures 7(a) and (b). Those obtained for the parabolic-nosed cylinder at an average wall-to-free-stream temperature ratio of 1.0 are shown in figure 7(c). Also included in figure 7 for comparison purposes are the laminar isothermal theory of Chapman and Rubesin (ref. 5) based on Eckert's (ref. 13) reference temperature, and the turbulent isothermal theory of Van Driest (ref. 6). The experimental data presented in figure 7 have not been corrected for the axial temperature distribution. The axial temperature distributions associated with these data are presented in table II.

Effect of Total Temperature

Experimental Stanton numbers were obtained for the conical section of the cone-cylinder model at total temperatures 523° and 630° R. These data corrected for the axial temperature distribution are presented in figure 8 and, as can be noted, the effect of changing the total temperature by this amount is negligible. Theoretically, no effect would be expected for an average wall-to-free-stream temperature ratio of 1.0. If the average temperature ratio is something other than 1.0, a small effect would be anticipated (approx. 1.5 percent for $T_w/T_0 \approx 2$).

Effect of Axial Temperature Distribution and Temperature Level

Representative laminar data for the cone-cylinder model at average wall-to-free-stream temperature ratios ranging from 1.0 to 4.4 are shown in figure 9 corrected for the axial temperature distribution according to equation (3). The first three or four data points at each Reynolds number per foot (see fig. 7) are moved downward by the temperature gradient correction. It should be noted here that what appeared to be an effect of Reynolds number per foot in the uncorrected data of figure 7(a) was actually the result of an axial temperature distribution. This comparison emphasizes the importance of accounting for the axial temperature distribution in calculating laminar-heat-transfer coefficients. As illustrated in figure 9, the corrected cone data agree closely with the theory at all temperature levels. However, if the fluid properties had not been evaluated at the reference temperature of reference 16, the experimental data for a temperature ratio of 4.0 would have been

approximately 20 percent higher than theory. Thus, when the reference temperature concept is used, it appears that both analytically and experimentally there is very little effect of surface temperature level on Stanton number.

Also included in figure 10 is a typical set of data (Re/ft = 4.5×10^6) obtained on the cylindrical section of the model. The data extend from a Reynolds number of 3.9×10^6 to 5.8×10^6. Note that the heat-transfer coefficients on the cylinder are lower than the cone values and approach the flat-plate values. This trend is to be expected and is predicted closely by the theory of reference 20, which is included in figure 9. The discontinuity existing in the heat-transfer rate is the result of the discontinuity in the pressure distribution.

An empirical method of predicting the isothermal cylindrical heat-transfer coefficients may be derived by calculating the heat-transfer coefficient just downstream of the cone-cylinder shoulder using the theory of reference 20 and by finding an equivalent two-dimensional heat-transfer coefficient. The free-stream cylindrical heat-transfer coefficient following the shoulder is given by

$$\left(\frac{St_{cy}}{St_c}\right)_s = \frac{\left(\frac{Nu}{\sqrt{Re_w}}\right)_{cy}}{\left(\frac{Nu}{\sqrt{Re_w}}\right)_c} \sqrt{\frac{(p_w u_1)_{cy}}{(p_w u_1)_c}} \tag{4}$$

Equation (4) reduces to

$$\left(\frac{St_{cy}}{St_c}\right)_s = \sqrt{\left(\frac{M_{cy}}{M_c}\right)^{B-1} \left(\frac{t_{1,cy}}{t_{1,c}}\right)^4 \frac{(p_w u_1)_{cy}}{(p_w u_1)_c}} = C \tag{5}$$

when the cylindrical pressure gradient is neglected and the ratio of specific heats is 1.4. For a given Mach number and cone angle, the Stanton number ratio in equation (5) is a constant. The quantities in equation (5) with the subscript cy are evaluated immediately downstream of the cone-cylinder juncture, whereas those with the subscript c are evaluated just upstream of the juncture. All terms appearing in equation (5), except the exponent B, may be evaluated from the pressure distribution. The exponent B may be found from figure 4 of reference 20.

The length of run (see following sketch) required to yield a two-

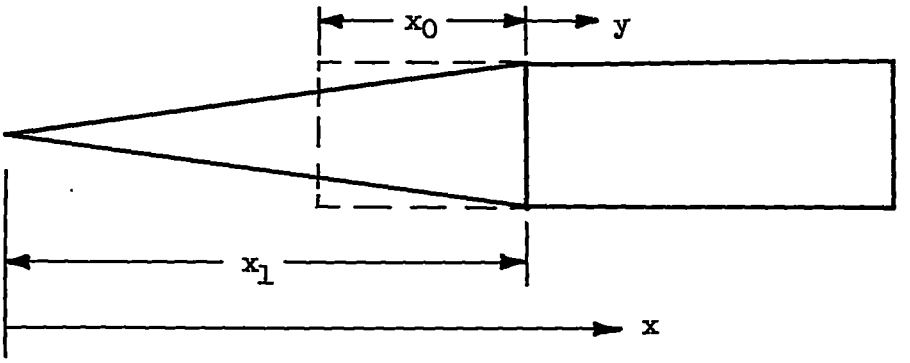

dimensional heat-transfer coefficient equal to the cylindrical coefficient defined in equation (5) is

$$x_0 = \frac{x_1}{3c^2}$$

The equivalent two-dimensional heat-transfer coefficient now becomes

$$St_{cy} = \frac{St_c}{\sqrt{3}\sqrt{1 - \frac{3c^2 - 1}{3c^2}\frac{x_1}{x}}} \tag{6}$$

where, for convenience, the length of run is defined in terms of x and x_1 rather than $x_0 + y$ (see preceding sketch). Observation of figure 10 shows that equation (6) predicts the same trend and about the same magnitude of the heat-transfer coefficients on the cylinder as reference 20. The use of equation (6) beyond the shoulder saves a considerable amount of time as compared with reference 20 with little sacrifice in accuracy.

Effect of Axial Pressure Distribution

A typical set of uncorrected data obtained from the parabolic-nosed cylinder is presented in figure 10, with the isothermal theory of reference 20. As expected, the theory does not predict the absolute value of the heat-transfer coefficient when the effect of temperature gradient is neglected. In fact, near the tip the experimental values are as much as 25 percent higher than the theoretical values. However, the effect of the temperature gradient may be accounted for approximately by assuming

the pressure and temperature effects to be independent. Consequently, it can be stated that

$$\left(\frac{h}{\bar{h}}\right)_p = \left(\frac{h}{\bar{h}}\right)_{fp} \tag{7}$$

where the ratio of the heat-transfer coefficients for the flat plate has been determined using the parabolic-cylinder-model temperature distribution converted to the equivalent two-dimensional values by the Mangler transformation (ref. 17). By accounting for the axial temperature distribution, the theory and experiment (fig. 10) now agree closely.

The local heat-transfer coefficients for the parabolic-nosed cylinder may also be calculated within 10 percent by considering the Mangler transformation and neglecting the axial pressure distribution (fig. 10). As a result, the ratio of the heat-transfer coefficient to the flat-plate coefficient becomes

$$\frac{St_0}{St_{fp}} = \sqrt{\frac{r^2 x}{\int_0^x r^2\, dx}} \sqrt{\frac{p_w u_1}{p_0 u_0}} \tag{8}$$

This was done previously for the cone-cylinder model with very little loss in accuracy. If the parabolic nosed section only is of interest, equation (5) will also predict the heat-transfer coefficients to within 10 percent. However, the use of equation (5) on the cylindrical section will give heat-transfer coefficients 10 to 21 percent higher than those predicted by the exact theory.

SUMMARY OF RESULTS

The following results were obtained from an investigation of the convective heat-transfer properties of two bodies of revolution at a Mach number of 3.12 and for Reynolds numbers to 12×10^6 based on model length:

1. Experimental laminar-heat-transfer coefficients obtained on the cone agreed closely with the theory of Chapman and Rubesin at all temperature levels when the fluid properties were based on Eckert's reference temperature. Also, experimentally and theoretically there was no significant effect of surface temperature level on the heat-transfer coefficient.

CU-2 back

2. Laminar-heat-transfer coefficients obtained from the cylindrical section of the cone-cylinder agreed closely with the theory of Cohen and Reshotko, which considers the pressure distribution. An empirical method of predicting the cylindrical heat-transfer coefficients was derived neglecting the cylindrical pressure gradient. The method saves a considerable amount of time with little sacrifice in accuracy.

3. The laminar data obtained from the parabolic-cylinder model agreed closely with the theory of Cohen and Reshotko when the data were corrected for the axial temperature distribution. The local heat-transfer coefficients for this model may also be predicted to within 10 percent by neglecting the axial pressure distribution and considering solely the Mangler transformation.

Lewis Flight Propulsion Laboratory
National Advisory Committee for Aeronautics
Cleveland, Ohio, July 5, 1956

APPENDIX A

SYMBOLS

The following symbols are used in this report:

A	model surface area, 0.48 sq ft
a	constant
C	constant
C_p	pressure coefficient
c_p	specific heat at constant pressure, Btu/(lb)(^oR)
h	local heat-transfer coefficient, Btu/(sec)(sq ft)(^oR)
$\overline{h}$	local heat-transfer coefficient for constant surface temperature
k	thermal conductivity
M	Mach number
Nu	Nusselt number
P'	total pressure
Pr	Prandtl number
p	local static pressure
Q	total heat-transfer rate
q	local heat-transfer rate per unit area
Re	Reynolds number, $Re_0 = \rho_0 u_0 x/\mu_0$
r	body radius
St	dimensionless heat-transfer coefficient, Stanton number, $St_0 = \frac{h}{\rho_0 c_{p,a} u_0}$
T	temperature
T'	total temperature, ^oR

t	time, sec
u	velocity
X	distance along model surface
x	axial distance, in.
ε	emissivity parameter
η	temperature recovery factor
μ	viscosity
ξ	dummy variable in x-direction (eq. (3))
ρ	density
σ	Boltzmann's constant, 0.173×10^{-8} Btu/(hr)(sq ft)($^{\circ}$R)^4
τ	wall thickness

Subscripts:

a	air
ad	adiabatic wall
b	model material
c	cone
cy	cylinder
fp	flat plate
p	parabolic
s	shoulder
T	tunnel wall
w	model wall
x	axial direction
0	free stream ahead of shock wave
1	edge of boundary layer

Superscripts:

B exponent

n number

APPENDIX B

RADIATION AND CONDUCTION EFFECTS

The determination of local heat-transfer coefficients from equation (2) assumes (1) no heat radiated from the tunnel walls to the model, (2) no axial conduction of heat, (3) zero heat transfer to the air inside the model, and (4) zero temperature gradient across the skin. A discussion of the validity of these assumptions is presented herein.

The heat transferred by radiation from the model to the tunnel walls was computed from the relation

$$Q = \sigma \varepsilon_{T,w} A (T_T^4 - T_w^4) \tag{B1}$$

If the radiating bodies are in the form of two coaxial cylinders the surfaces of which radiate diffusely, the expression for $\varepsilon_{T,w}$ becomes

$$\varepsilon_{T,w} = \frac{1}{\frac{1}{\varepsilon_w} + \left(\frac{1}{\varepsilon_T} - 1\right)\frac{A}{A_T}} \tag{B2}$$

where A_T is the tunnel radiating area. Since the wind tunnel walls are fabricated from stainless steel and the models were made from monel, the values for the respective emissivities are taken to be 0.4 and 0.09. This results in $\varepsilon_{T,w}$ equal to 0.089.

The condition under which the largest amount of heat is radiated exists for a hot model at the lowest Reynolds number per foot. Using 772° R for T_w and a turbulent recovery temperature of 493° F at the tunnel wall results in a total heat-transfer rate Q equal to 0.006 Btu per second. Comparing this value with the average rate of heat transfer by convection ($Q = 0.294$ Btu/sec) shows that the former is approximately 2.0 percent of the latter. However, for all other test conditions, the error was less than 1.5 percent and was neglected.

The assumption of zero axial heat transfer was investigated by considering the most severe axial temperature distribution available at any of the temperature ratios reported. Under these conditions, the axial heat-conduction terms in equation (1) were evaluated. A comparison of the heat-transfer rates due to conduction and to convection indicated the former to be less than ± 2 percent of the latter. As a consequence, the axial conduction terms in equation (1) were neglected in the computations of heat transfer.

The third source of error considered was the heat transferred from the model to the inside air by conduction. Temperature-time histories at various points within a model were recorded during a test run. From this an average heat-transfer coefficient can be computed if the total heat input over a finite time interval is known. The results of such a calculation indicate that the heat loss to the inside of the model is always less than 1/2 percent.

As mentioned in the report, the convective heat-transfer coefficient was computed from equation (2) which assumes a very thin model skin. This means zero temperature gradient in the direction normal to the flow. While the test models did not meet this specification rigorously, it can be shown that the discrepancy in the heat-transfer calculation is unimportant. Consider the section abcd of the model wall shown in the following sketch:

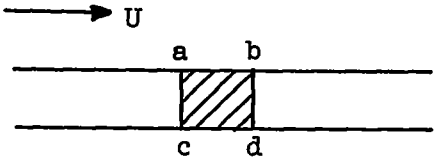

As has been discussed previously, the heat transferred across the boundaries ac and bd is negligible. Knowing this fact, the temperature profile across the skin may be calculated. Heat was considered to flow into the area in such a manner that the boundary ab experienced an exponential temperature rise. The actual temperature-time history used was that of a typical model thermocouple. The analysis indicated that the temperature was constant in the y-direction to within 1 percent of the measured value. Consequently, the error incurred by the use of the thin-shell concept for the heat-transfer computations is trivial.

APPENDIX C

EFFECT OF CONDENSATION ON HEAT TRANSFER

Since the physical characteristics of the condensation film are not known, the absolute error due to condensation can not be estabilished. Its order of magnitude may, however, be estimated.

First, the actual mechanism of condensation with the subsequent evaporation is considered in relation to the model temperature. A component of the air stream, upon condensing at a given axial station, will release heat, thus causing the temperature to increase locally. The condensate will remain on the body and be heated as the body temperature continues to rise. Subsequently, the film will reach its boiling point, acquire its heat of vaporization, and evaporate. Thus, if the quantities of heat considered previously are significant, it is anticipated that the model temperature would be influenced. At any rate, a noticeable difference in the time rate of change of temperature should be observed. A temperature history of the following type would be expected at any given thermocouple location:

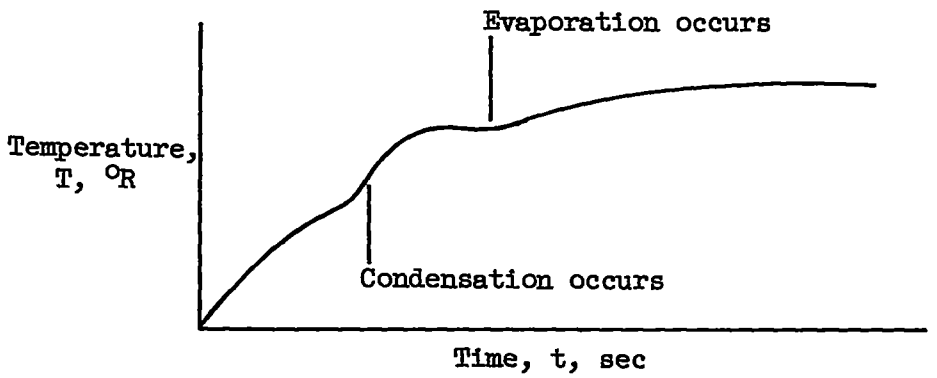

A careful examination of the oscillograph traces does not reveal this type of temperature distribution.

Any appreciable effect of a condensation film should also be observed in a plot of heat-transfer coefficient against Reynolds number for various times or temperature ratios. These plots have been made for the cone-cylinder model at wall-to-free-stream temperature ratios ranging from 1.0 to 4.0 (fig. 10). The data presented for temperature ratios from approximately 1.0 to 1.7 were obtained with and without condensation; whereas, data for the higher temperature ratios were obtained without condensation. Since the heat-transfer coefficient is directly dependent on the time rate of change of temperature, a comparison of these data should show different variations with time. However, observation of figure 10 indicates no systematic variation of the heat-transfer coefficient with time for either the hot or cold model.

Although neither of the two arguments presented concerning the condensation phenomenon are decisive, they are physically reasonable. Consequently, since the two effects discussed previously were not observed in the experimental data, it was concluded that the determination of local heat-transfer coefficients was not significantly influenced by the condensation phenomenon.

REFERENCES

1. Scherrer, Richard: Comparison of Theoretical and Experimental Heat-Transfer Characteristics of Bodies of Revolution at Supersonic Speeds. NACA Rep. 1055, 1951. (Supersedes NACA RM A8L28; TN's 1975, 2087, 2131, and 2148.)

2. Eber, G. R.: Recent Investigation of Temperature Recovery and Heat Transmission on Cones and Cylinders in Axial Flow in the N.O.L. Aeroballistics Wind Tunnel. Jour. Aero. Sci., vol. 19, no. 1, Jan. 1952, pp. 1-6.

3. DeCoursin, D. G., Bradfield, W. S., and Sheppard, J. J.: Aerodynamic Heating and Heat Transfer Phenomena at Mach Numbers 4 Through 5.7. Res. Rep. No. 101. Inst. Tech., Dept. Aero. Eng., Rosemount Aero. Labs., Univ. of Minn., Feb. 1954. (USAF Contract AF 35(038)10673.)

4. Van Driest, E. R.: Investigation of Laminar Boundary Layer in Compressible Fluids Using the Crocco Method. NACA TN 2597, 1952.

5. Chapman, Dean R., and Rubesin, Morris W.: Temperature and Velocity Profiles in the Compressible Laminar Boundary Layer with Arbitrary Distribution of Surface Temperature. Jour. Aero. Sci., vol. 16, no. 9, Sept. 1949, pp. 547-565.

6. Van Driest, E. R.: Turbulent Boundary Layer in Compressible Fluids. Jour. Aero. Sci., vol. 18, no. 3, Mar. 1951, pp. 145-161.

7. Jack, John R., and Diaconis, N. S.: Variation of Boundary-Layer Transition with Heat Transfer on Two Bodies of Revolution at a Mach Number of 3.12. NACA TN 3562, 1955.

8. Van Dyke, Milton S.: Practical Calculation of Second-Order Supersonic Flow Past Nonlifting Bodies of Revolution. NACA TN 2744, 1952.

9. Ladenberg, R., Van Voorhis, C. C., and Winckler, J.: Interferometric Study of Supersonic Phenomena. Pt. II - The Gas Flow Around Various Objects in a Free Homogeneous Supersonic Air Stream. NAVORD Rep. 93-46, Bur. Ord., Navy Dept., Sept. 2, 1946.

10. Hampton, W. F., and Mennie, J. H.: The Specific Heat of Monel Metal Between -183° and 25° C. Canadian Jour. Res., vol. 7, July-Dec. 1932, pp. 677-678; discussion, pp. 678-679.

11. Douglas, Thomas B., and Dever, James L.: Enthaply and Specific Heat of Four Corrosion-Resistant Alloys at High Temperatures. Jour. Res. Nat. Bur. Standards, vol. 54, no. 1, Jan. 1955, pp. 15-19.

12. Glasstone, Samuel: Textbook of Physical Chemistry. Second ed., D. Van Nostrand Co., Inc., 1946, p. 415.

13. Eckert, E. R. G.: Engineering Relations for Friction and Heat Transfer to Surfaces in High Velocity Flow. Jour. Aero. Sci., vol. 22, no. 8, Aug. 1955, pp. 585-586.

14. Young, George B. W., and Janssen, Earl: The Compressible Laminar Boundary Layer. Jour. Aero. Sci., vol. 19, no. 4, Apr. 1952, pp. 229-236.

15. Klunker, E. B., and McLean, F. Edward: Laminar Friction and Heat Transfer at Mach Numbers from 1 to 10. NACA TN 2499, 1951.

16. Moore, L. L.: A Solution of the Laminar Boundary-Layer Equations for a Compressible Fluid with Variable Properties, Including Dissociation. Jour. Aero. Sci., vol. 19, no. 8, Aug. 1952, pp. 505-518.

17. Mangler, W.: Compressible Boundary Layers on Bodies of Revolution. VG 83, No. 47T, M.A.P. Volkenrode.

18. Lighthill, M. J.: Contributions to the Theory of Heat Transfer Through a Laminar Boundary Layer. Proc. Roy. Soc. (London), ser. A, vol. 202, no. A1070, Aug. 7, 1950, pp. 359-377.

19. Shoulberg, Robert H., Kendall, Robert E., and Finston, Morton: An Experimental Investigation of Flat Plate Heat Transfer Coefficients at Mach Numbers of 2, 2.5, and 3 for a Surface Temperature to Stream Total Temperature of 1.18. Wind Tunnel Rep. No. 39, Naval Supersonic Lab., M.I.T., June 1953. (USAF Contract No. AF 33(038)-23165.)

20. Cohen, Clarence B., and Reshotko, Eli: The Compressible Laminar Boundary Layer with Heat Transfer and Arbitrary Pressure Gradient.

TABLE I. - COMPOSITION OF NICKEL ALLOYS

Material	Composition, percent	
	Monel	"K" monel
Nickel	65.98	64.35
Copper	29.75	29.58
Iron	1.40	1.00
Manganese	.90	.60
Aluminum	.40	3.40
Carbon	.15	.13
Silicon	.10	.03
Sulfur	.01	.008

TABLE II. - AXIAL TEMPERATURE DISTRIBUTIONS (Figs. 7 and 8)

(a) Cone-cylinder model.

Axial distance, x, in.	Cold				
	Axial temperature, T_x, °R				
	Total temperature, T', °R				
	524	515	631	630	523
	Reynolds number per foot, Re				
	8×10^6	4.5×10^6	2.25×10^6	1.25×10^6	1.25×10^6
2	338.5	296.3	329.0	290.5	245.9
3	298.3	263.0	291.0	256.5	220.7
4	276.8	242.0	266.5	234.5	205.0
5	263.4	229.3	249.5	219.5	196.1
6	255.2	213.0	239.0	208.5	189.2
7	251.0	215.8	231.5	203.0	184.8
8	252.4	217.1	233.5	217.0	187.3
9	252.5	217.0	232.0	214.5	185.9
10	258.9	214.9	228.5	213.0	182.8
10.62	254.0	214.4	223.5	210.0	178.9
11.5	251.5	202.5	218.5	206.0	175.9
12.5	260.6	199.9	215.0	202.5	168.5
13.62	279.5	206.0	215.0	196.0	-----
14.75	-----	-----	205.0	218.0	169.2
16	291.5	200.2	-----	-----	-----

Axial distance, x, in.	Hot				
	Axial temperature, T_x, °R				
	Total temperature, T', °R				
	522	532	532	532	532
	Reynolds number per foot, Re				
	8×10^6	6.75×10^6	4.5×10^6	2.25×10^6	1.25×10^6
2	597.8	-----	690.9	723.0	743.8
3	589.0	626.4	709.0	748.3	764.5
4	591.5	610.0	684.9	758.3	772.0
5	610.3	624.0	660.4	760.0	773.4
6	613.0	-----	661.9	752.8	773.9
7	617.5	628.4	663.9	734.0	769.9
8	620.3	628.0	664.8	717.3	766.1
9	624.0	633.0	666.3	713.0	766.0
10	623.8	633.1	667.5	710.0	755.7
10.62	638.9	645.0	678.5	717.5	752.0
11.5	645.8	653.9	687.3	728.0	751.9
13.62	637.9	643.0	678.2	718.8	740.2
14.75	641.2	647.0	678.9	716.0	726.7

TABLE II. - Concluded. AXIAL TEMPERATURE DISTRIBUTIONS (Figs. 7 and 8)

(b) Parabolic-nosed-cylinder model.

Axial distance, x, in.	Axial temperature, T_x, °R					
	Stagnation temperature, T', °R					
	522	522	630	630	630	520
	Reynolds number per foot, Re					
	8×10^6	4.5×10^6	4.5×10^6	2.25×10^6	1.25×10^6	1.25×10^6
1	392.5	356.9	442.6	294.7	194.8	291.8
1.5	358.7	321.8	398.3	350.8	328.6	261.5
2	340.2	303.6	374.0	328.6	297.3	246.7
3	307.6	273.5	331.1	291.5	266.8	220.8
4	296.5	261.4	311.0	274.4	249.8	212.4
5	282.6	246.5	294.6	259.0	237.4	200.4
6	273.6	237.4	283.9	248.7	226.3	193.2
7	265.5	228.5	271.2	238.6	216.5	186.0
8	261.1	220.6	261.3	233.5	-----	180.6
9	256.8	214.5	255.5	224.6	206.0	176.3
10	250.8	206.8	243.7	215.7	201.9	172.4
11	252.6	203.0	236.2	211.2	201.6	169.2
12.5	261.3	204.2	230.7	206.7	-----	172.8
16	-----	208.5	235.3	210.5	-----	-----

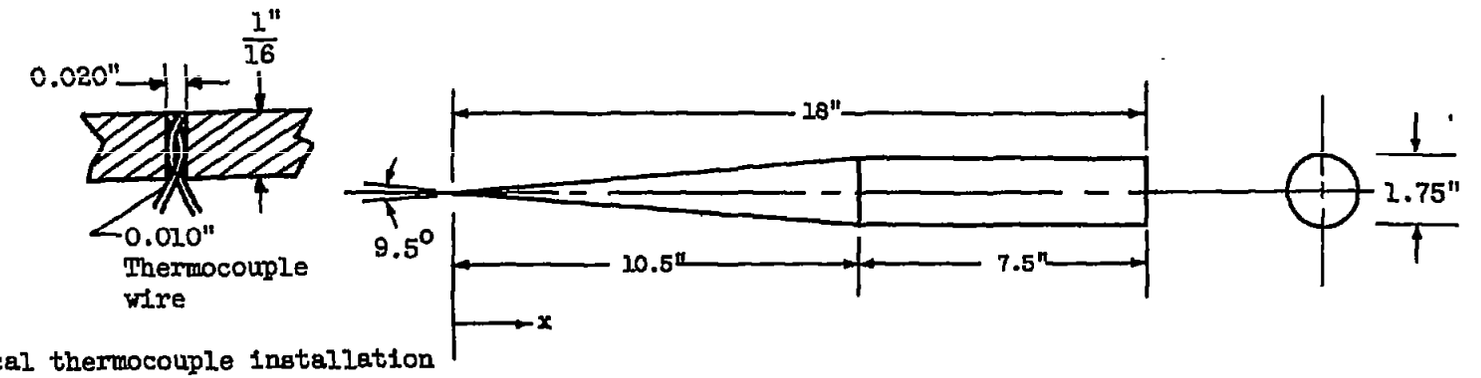

Typical thermocouple installation

Thermocouple locations at axial distance, x, in.														
2.0	3.0	4.0	5.0	6.0	7.0	8.0	9.0	10.0	10.62	11.50	12.50	13.62	14.75	16.00

(a) Cone-cylinder model.

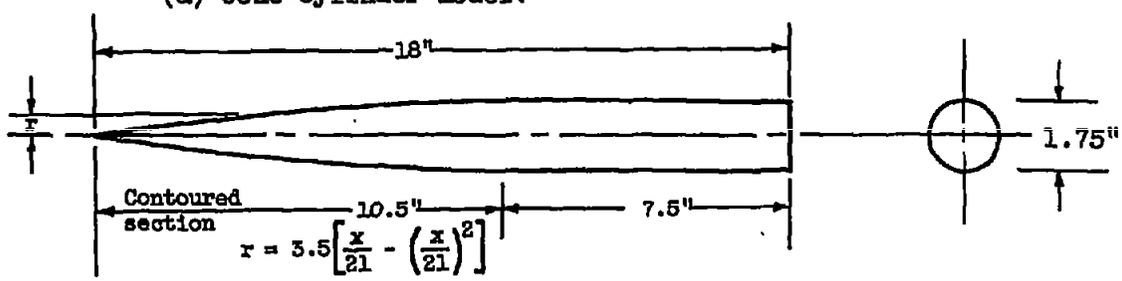

Thermocouple locations at axial distance, x, in.														
1.0	1.5	2.0	3.0	4.0	5.0	6.0	7.0	8.0	9.0	10.0	11.0	12.5	14.0	16.0

(b) Parabolic-nosed-cylinder model.

Figure 1. - Details of models and thermocouple locations.

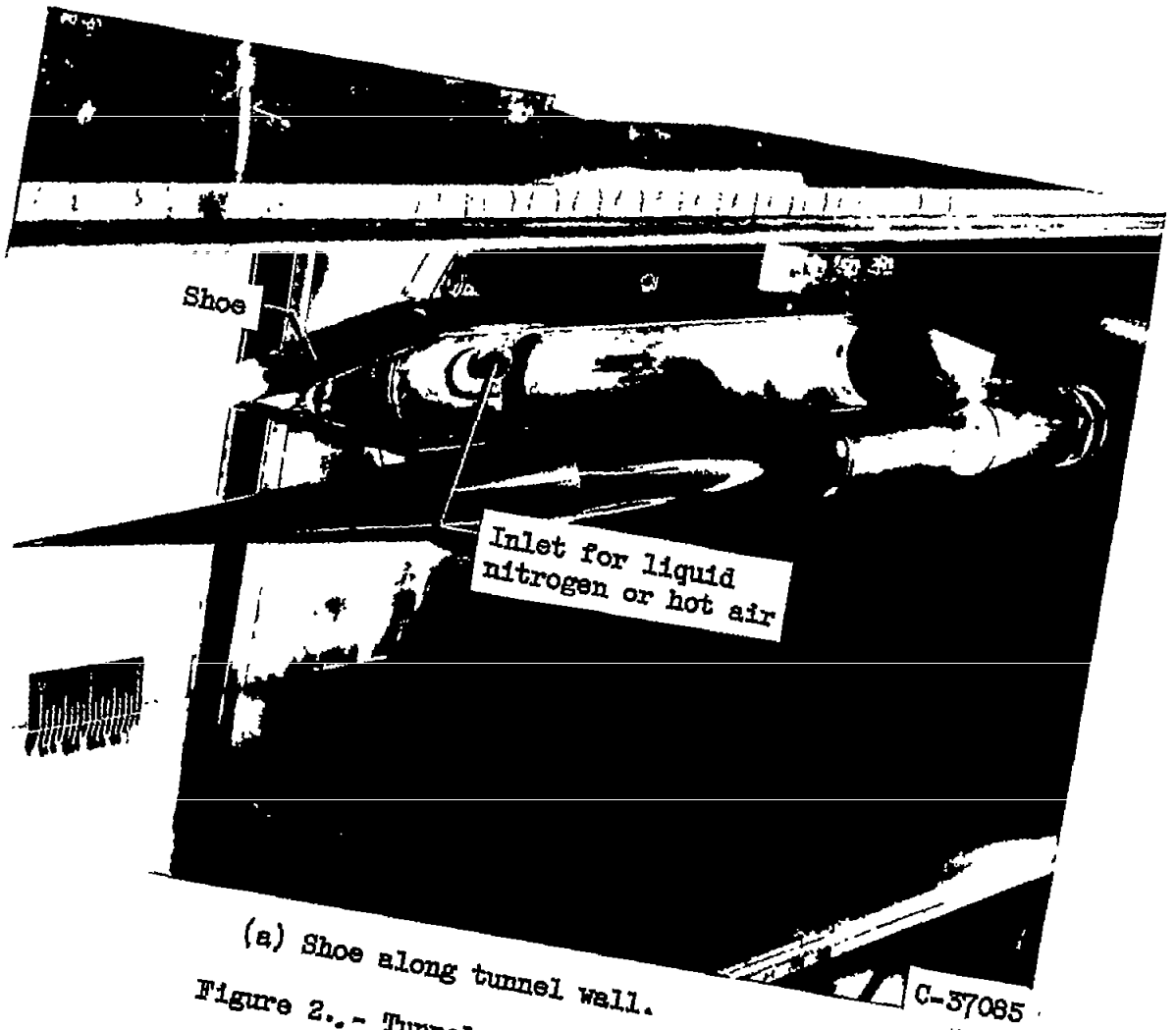

(a) Shoe along tunnel wall.

Figure 2.- Tunnel installation.

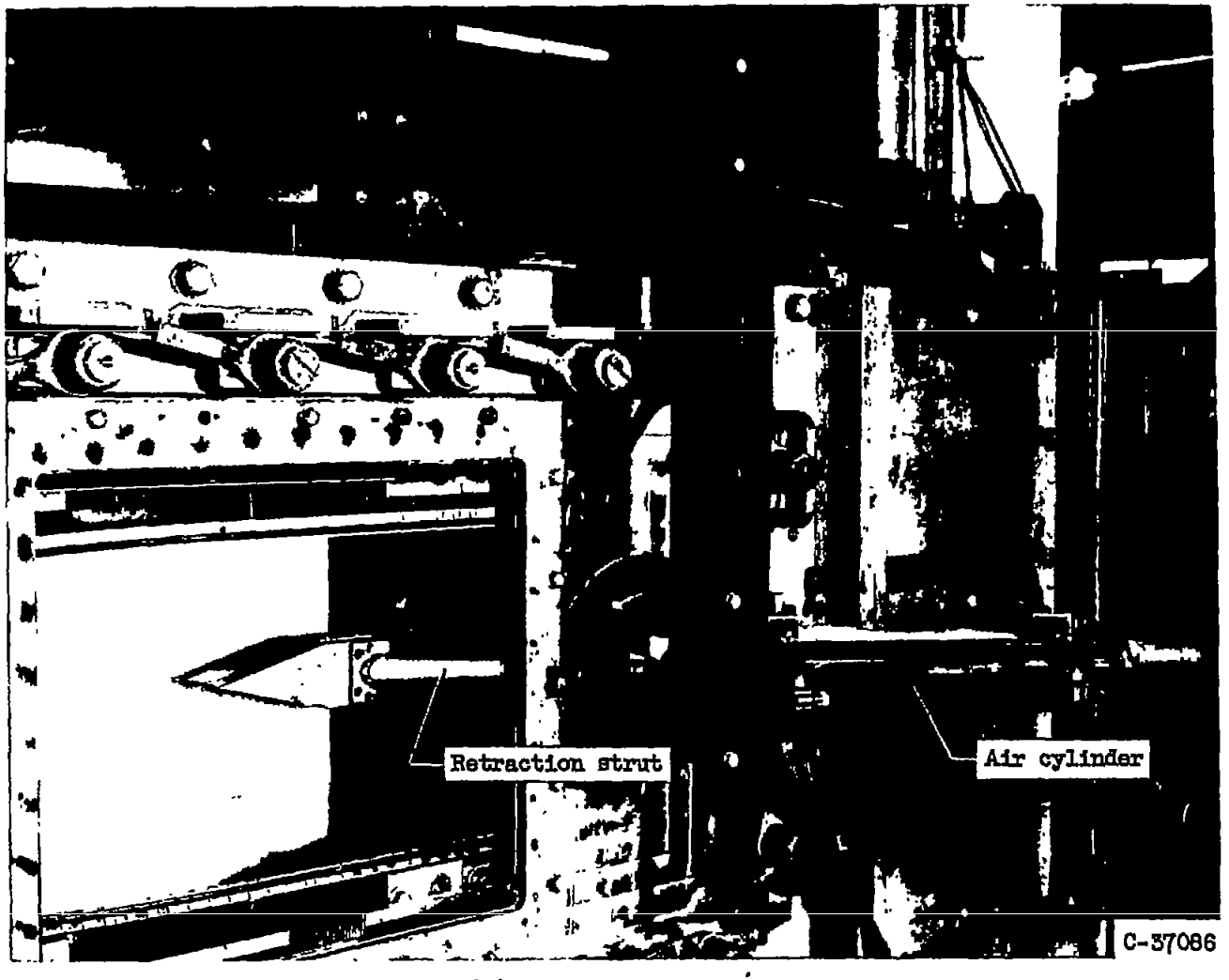

(b) Shoes in place.

Figure 2. - Tunnel installation.

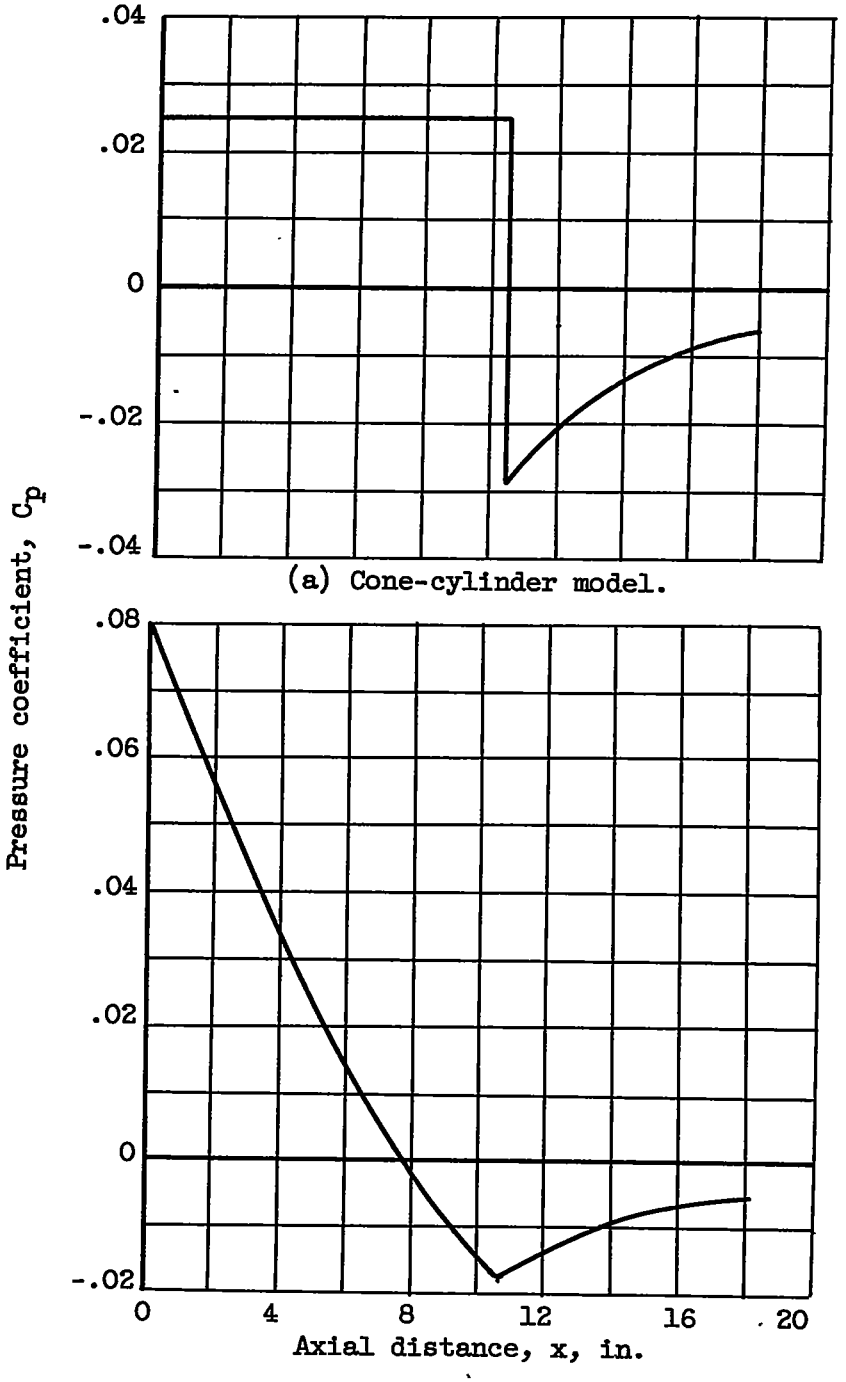

(a) Cone-cylinder model.

(b) Parabolic-nosed-cylinder model.

Figure 3. - Surface-pressure distribution for two bodies of revolution at zero angle of attack.

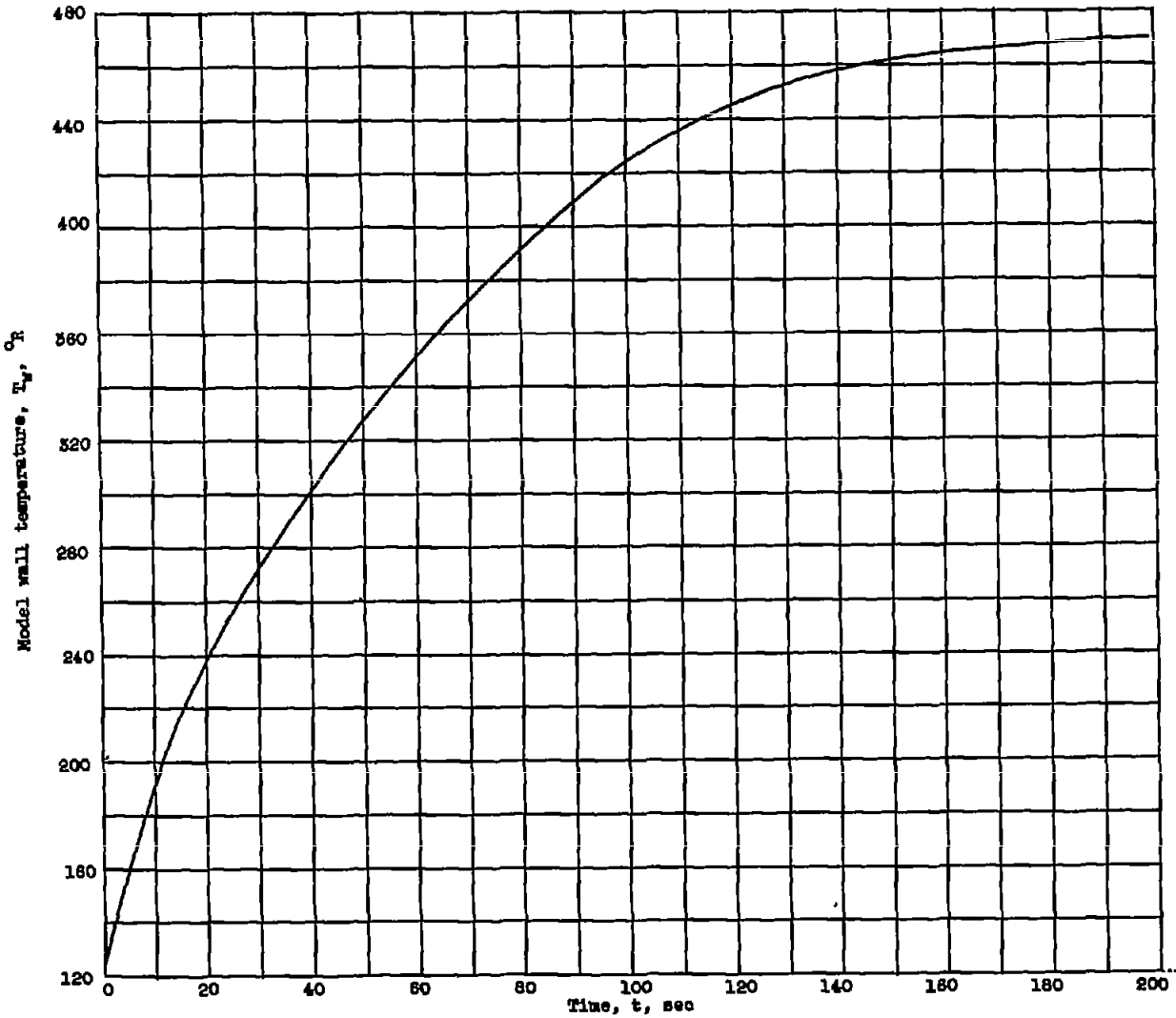

Figure 4. - Typical temperature history for cooled cone. Total temperature, 524° R; Reynolds number per foot, 8×10^6; axial distance, 4 inches.

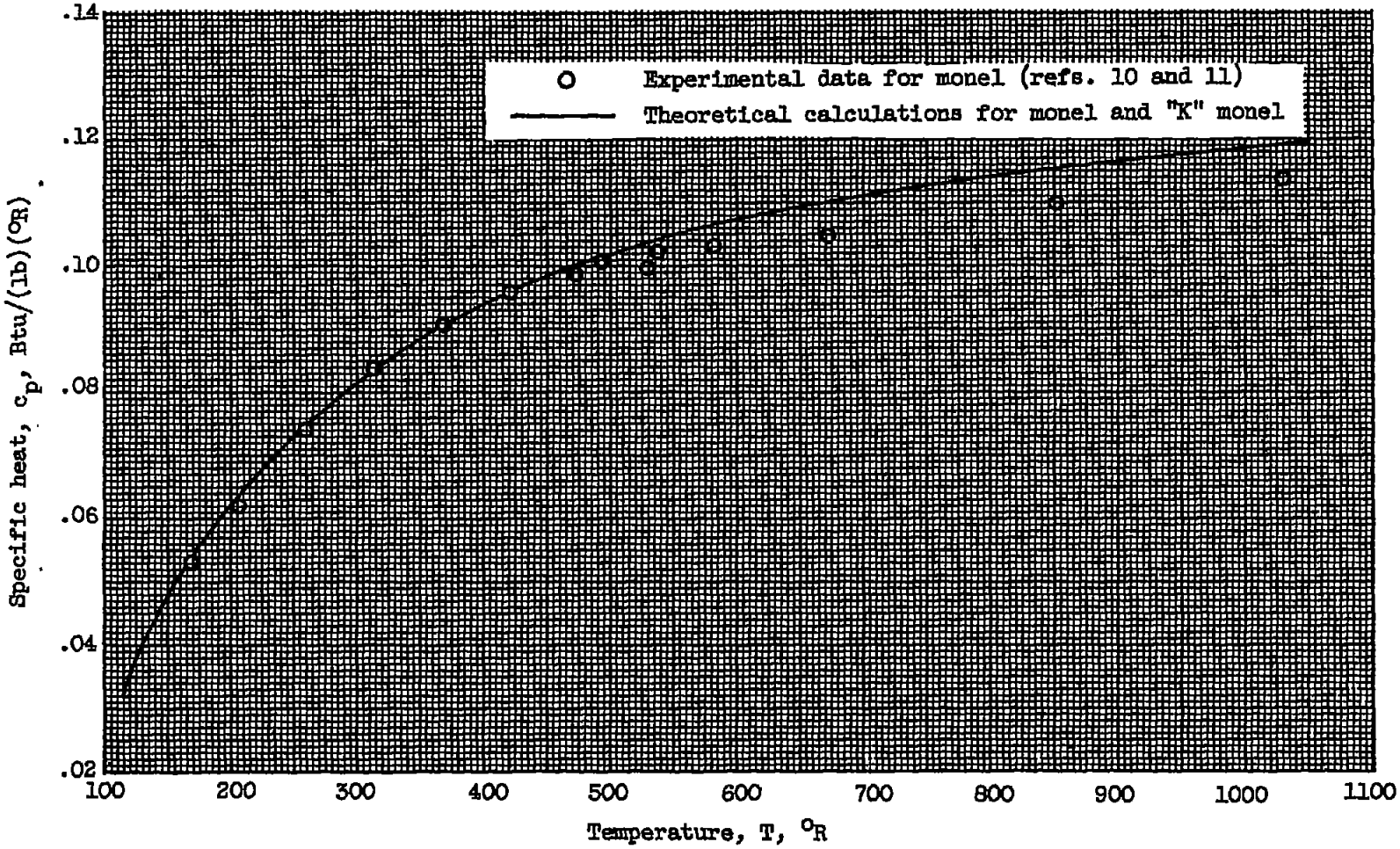

Figure 5. - Variation of specific heat with temperature.

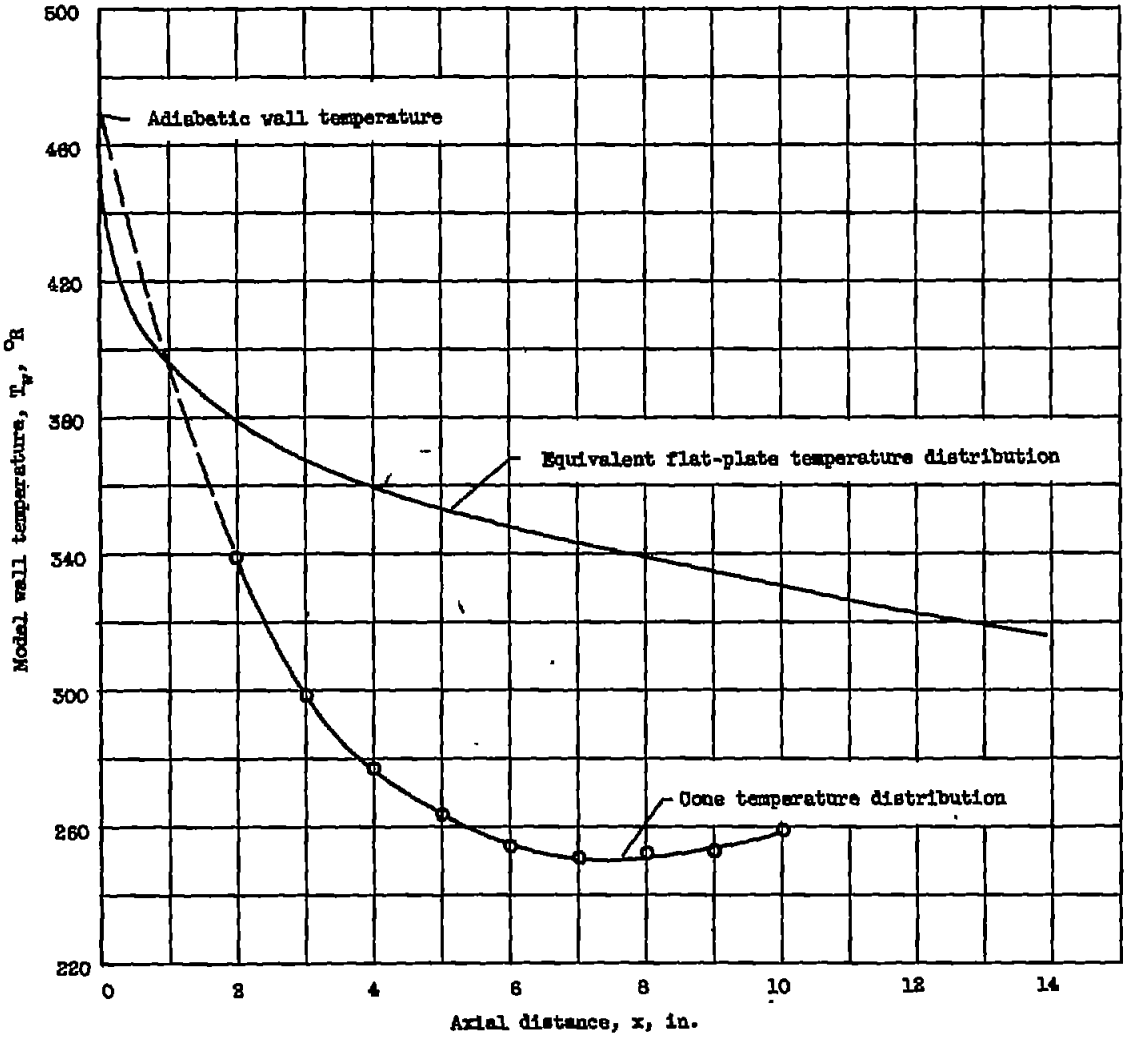

Figure 6. - Typical axial temperature distributions. Total temperature, 524° R; Reynolds number per foot, 8×10^6.

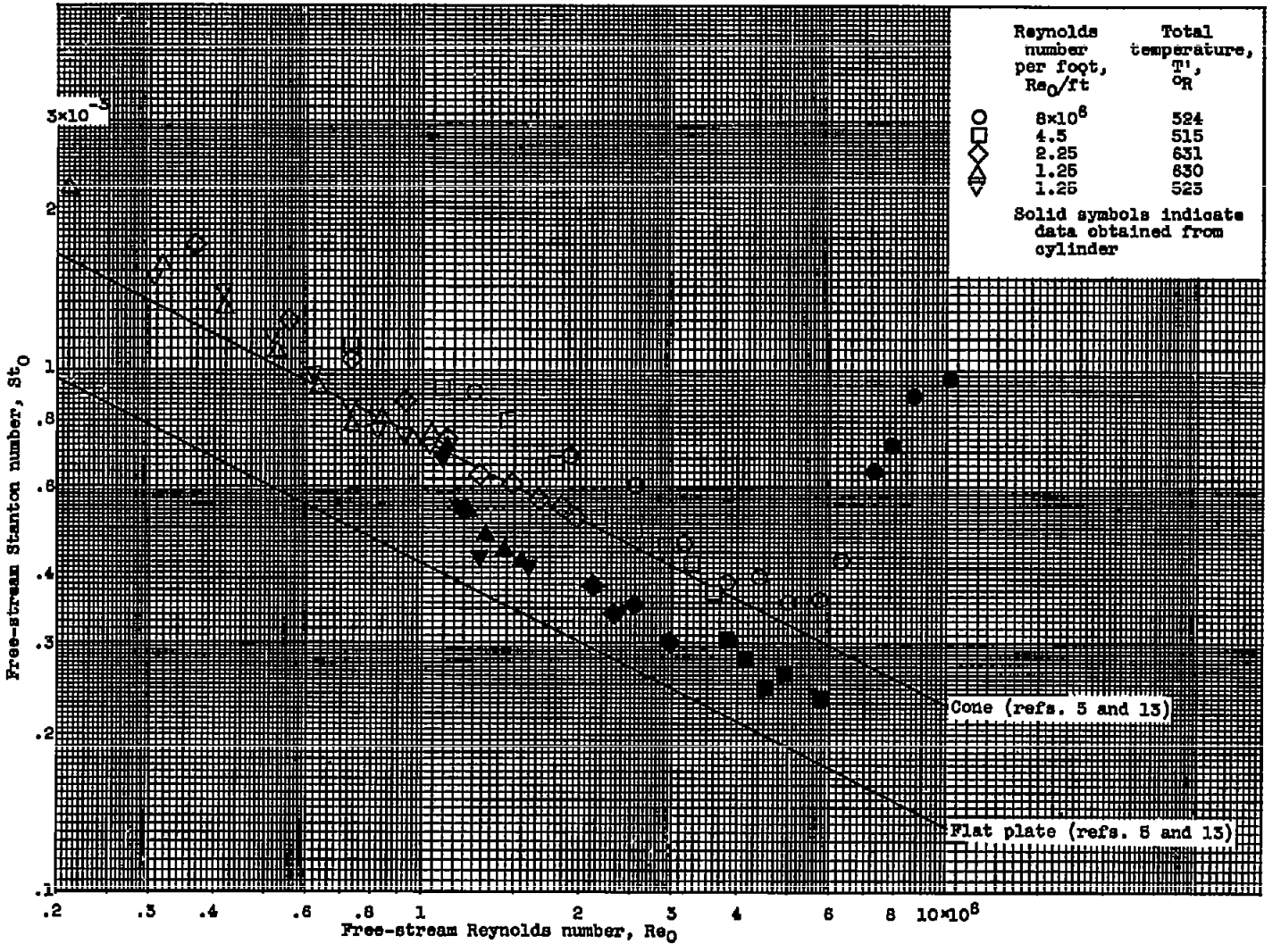

(a) Cold cone-cylinder model; initial temperature, 120° R; wall-to-free-stream temperature ratio, 1.0.

Figure 7. - Local laminar-heat-transfer coefficients at Mach number of 3.12.

(b) Hot cone-cylinder model; initial temperature, 780° R; wall-to-free-stream temperature ratio, 4.0.

Figure 7. - Continued. Local laminar-heat-transfer coefficients at Mach number of 3.12.

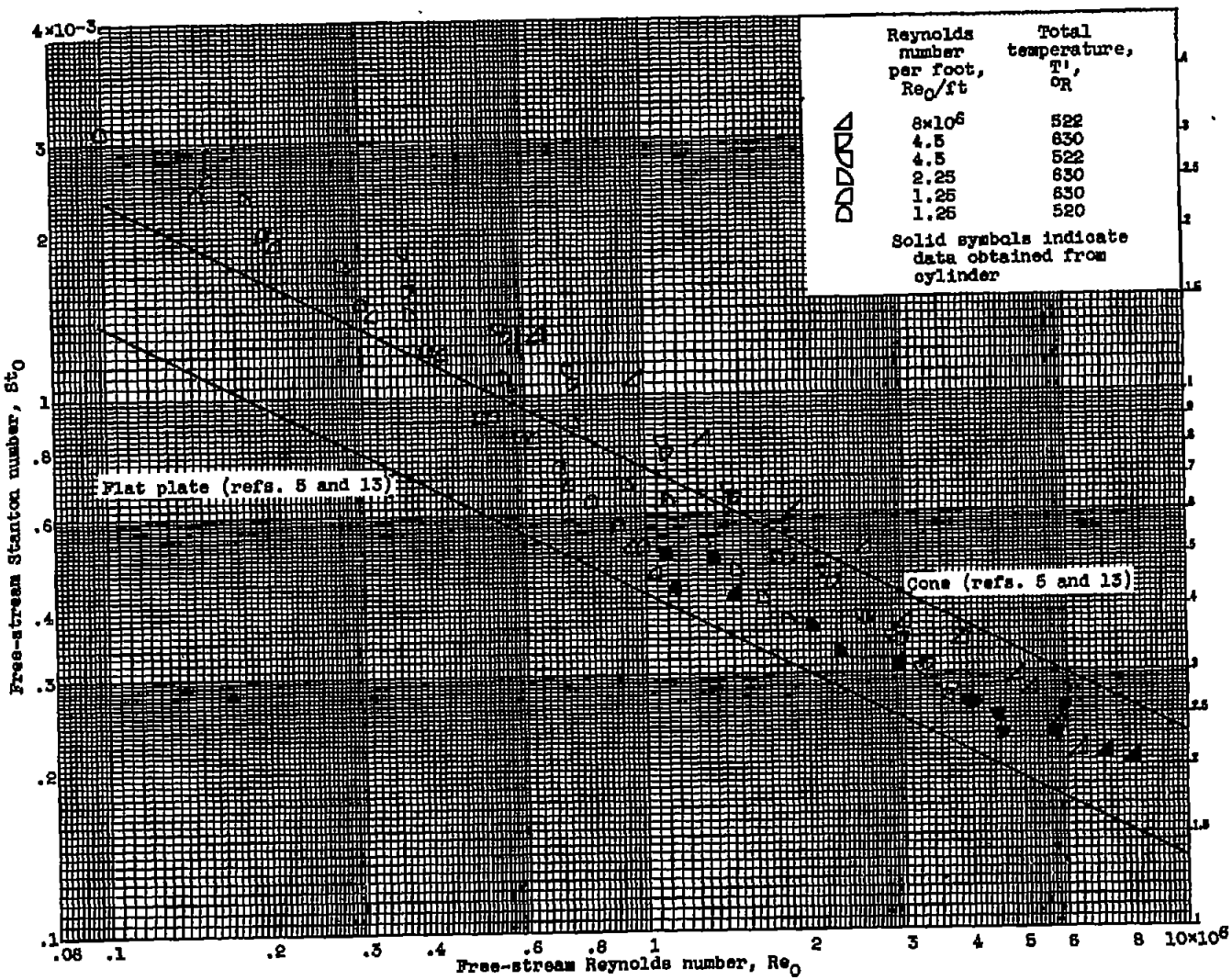

(c) Cold parabolic-nosed-cylinder model; initial temperature, 120° R; wall-to-free-stream temperature ratio, 1.0.

Figure 7. - Concluded. Local laminar-heat-transfer coefficients at Mach number of 3.12.

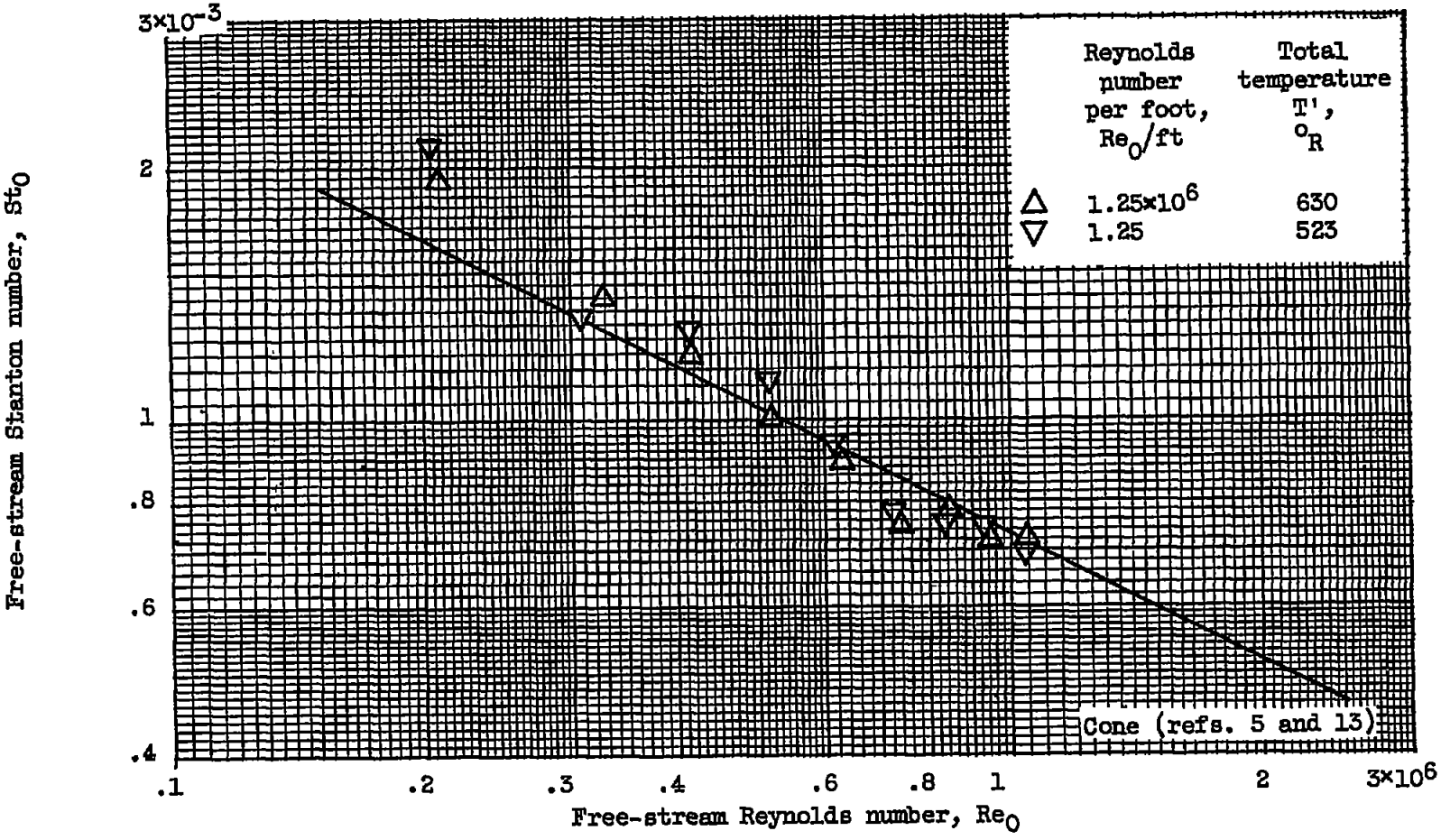

Figure 8. - Effect of tunnel total temperature on local laminar-heat-transfer coefficients on cone-cylinder model. Initial temperature, 120° R; wall-to-free-stream temperature ratio, 1.0.

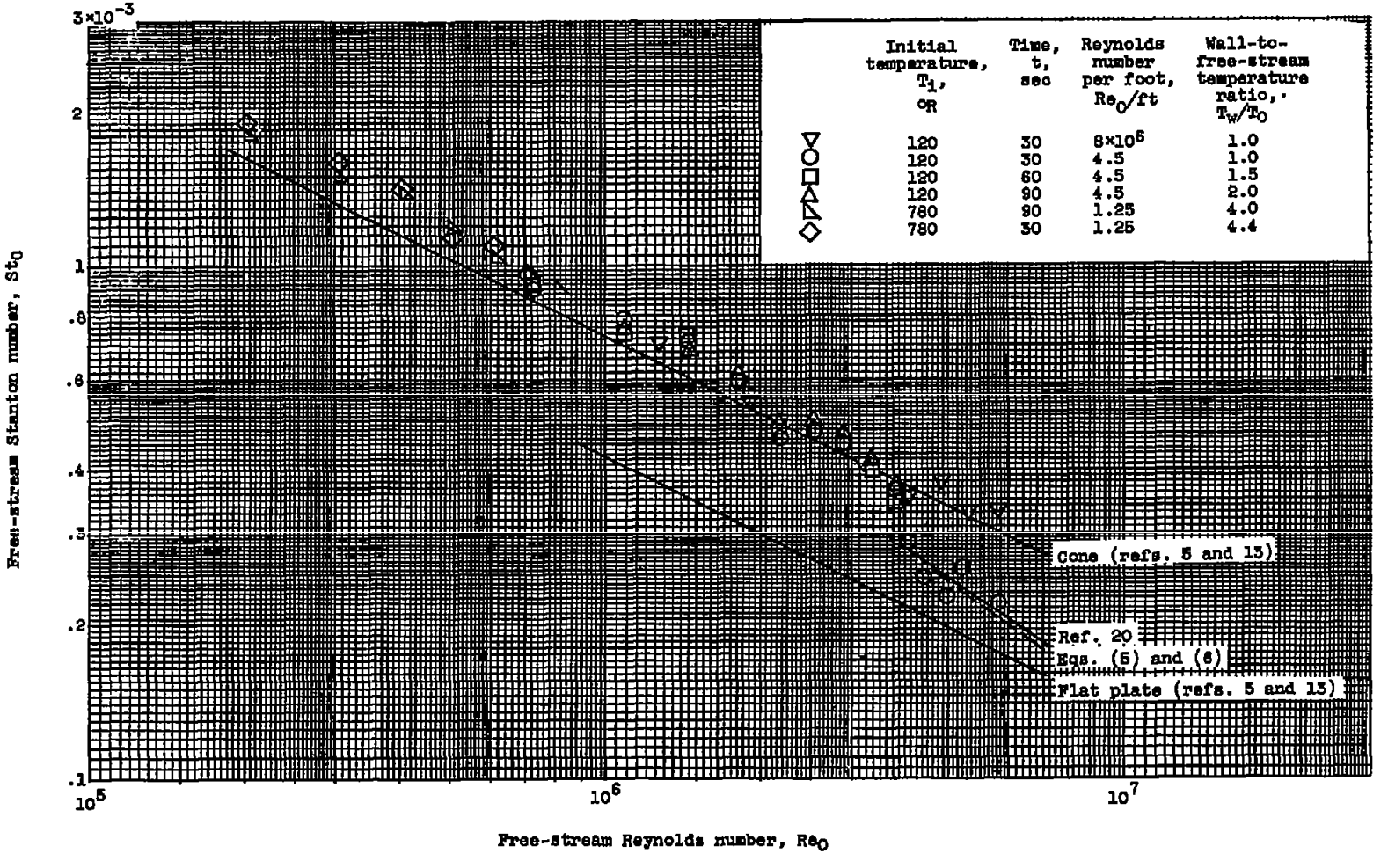

Figure 9. - Effect of temperature ratio on local laminar-heat-transfer coefficients on cone-cylinder model. Total temperature, 515° to 523° R.

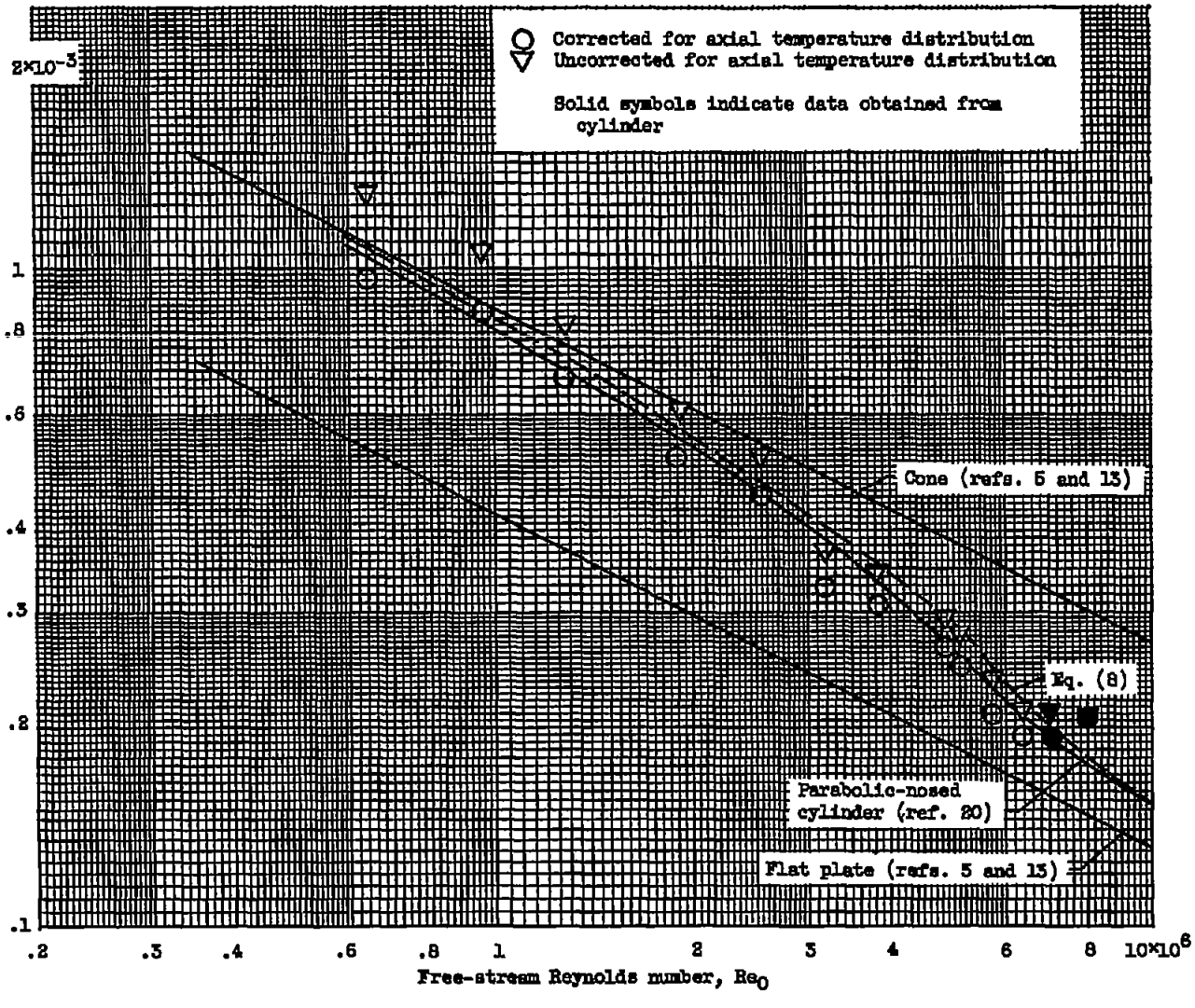

Figure 10. - Local laminar-heat-transfer coefficients on parabolic-nosed cylinder model. Initial temperature, 120° R; total temperature, 522° R; Reynolds number per foot, 8×10^6.